

Late Oligocene–early Miocene transformation of postcollisional magmatism in Tibet

Zhengfu Guo^{1,2*} and Marjorie Wilson³¹Key Laboratory of Cenozoic Geology and Environment, Institute of Geology and Geophysics, Chinese Academy of Sciences (CAS), Beijing 100029, China²CAS Center for Excellence in Life and Paleoenvironment, Beijing 100044, China³School of Earth and Environment, University of Leeds, Leeds LS2 9JT, UK

ABSTRACT

Uplift of the Tibetan Plateau is thought to be one of the most important orogenic and climate forcing events of the Cenozoic Era, associated with geodynamic changes related to India-Asia collision and subsequent continental lithosphere subduction. However, the fate and scale of the subducted continental lithosphere segments remain highly controversial. Using a comprehensive compilation of the spatiotemporal distribution of postcollisional magmatic rocks across Tibet, together with new geochemical and Sr-Nd-Pb isotopic data and modeling simulations, we propose a holistic, two-stage evolutionary model to explain the link between genesis of the magmas and continental subduction. The magmatism prior to 25 Ma resulted from continuous upwelling of a carbonate-rich upper-mantle plume induced by northward underthrusting of Indian oceanic and continental lithosphere with its cover of Tethyan platform carbonate sediments, whereas magmatism after 25 Ma was related to opposing north-directed and south-directed continental subduction. Our model indicates a transformation in the distribution and nature of the magmatism in Tibet at ca. 25 Ma, which reflects a significant change in the Himalayan-Tibetan orogen and associated mantle dynamic processes in the early Miocene. Understanding this transformation could have important implications for the utility of the Himalayan-Tibetan system as a modern analogue for ancient orogens.

INTRODUCTION

Tibetan Plateau uplift is one of the most important Cenozoic geological events (DeCelles et al., 2014), and it is considered to be the topographic expression of northward Indian plate subduction (Replumaz et al., 2016). However, the timing and location of the northern leading edge of continental lithosphere subduction have been topics of vigorous debate (Chen et al., 2018).

Understanding the petrogenesis of postcollisional magmatism can provide important constraints on the processes of continental subduction (Guo et al., 2015). Previous studies have focused on individual volcanic fields, with limited sampling of the regional distribution of magmatism (Williams et al., 2001), and their petrogenesis has not been fully investigated in a geodynamic context. Almost all previous studies were based on differentiated magmatic rocks (MgO < 6 wt%), the parental magmas of which may have undergone combined crustal assimilation and frac-

tional crystallization (AFC), making it difficult to understand the characteristics of their mantle source (Guo et al., 2006). Lack of detailed field sampling and of petrological, geochronological, and geochemical data has precluded further constraints on the petrogenesis of the magmas and their link to continental subduction. By constraining the compositional characteristics of primitive postcollisional magmatic rocks across the whole Tibetan Plateau (Fig. 1), we developed a robust model to better explain the link between continental subduction and magma petrogenesis.

GEOLOGICAL SETTING

The Tibetan Plateau is a collage of nearly east-west-trending allochthonous terranes, including the Songpan-Ganzi, Qiangtang, and Lhasa terranes, from north to south. These terranes are bounded by a series of tectonic sutures (Fig. 1). The Jinsha, Kunlun, and Bangong-Nujiang sutures resulted from Tethys oceanic closures, whereas the Indus-Tsangpo suture marks the boundary of India-Asia collision at 65–60 Ma, according to re-

cent studies (DeCelles et al., 2014; Hu et al., 2015). Postcollisional magmatism has occurred across the whole plateau, with a near-continuous range of igneous activity since 55 Ma (Table DR1 in the GSA Data Repository¹). Based on our compilation of ages for volcanism (Table DR1), this may be subdivided into two stages, which may be further subdivided into groups 1–3 (Fig. 1). The early stage (group 1) formed large-scale lava flows and pyroclastic deposits in central Tibet (55–25 Ma); the late stage is distributed in southern (group 2; 25–8 Ma) and northern (group 3; 25 Ma–present) Tibet (Fig. 2A), where small-scale lava flows occur within extensional basins. The age and volume of the magmatism decrease from central (pre–25 Ma) to south and north Tibet (post–25 Ma); the compositions of the magmatic rocks also change from central to south and north Tibet (Figs. 2 and 3).

COMPOSITION OF GROUP 1–3 ROCKS

Whole-rock major- and trace-element and Sr-Nd-Pb isotope data for groups 1–3 were obtained for 91 primitive (MgO > 6 wt%) magmatic rocks from across the whole of Tibet (Table DR4). They are not affected by crustal contamination (AFC), as evidenced by a lack of correlation of ⁸⁷Sr/⁸⁶Sr with SiO₂, and therefore may provide important constraints on the nature of their mantle source. Geochemical modeling allowed us to quantify the relative roles of carbonatitic melts and subducted terrigenous sediments in their mantle source (Fig. 3C).

Group 1 includes ultrapotassic, potassic, high-K calc-alkaline (HKCA), and Na-rich rocks, forming a continuous suite from K-rich to Na-rich magmatic rocks in central Tibet (Figs. 1 and 2B). The samples display elevated CO₂ contents in melt inclusions within pyroxene phenocrysts (Figs. DR1–DR3). They have low Ni/MgO and SiO₂ contents (Fig. 2D) and high Ca in olivine phenocrysts (Fig. 3A). Group 1 exhibits decreas-

*E-mail: zfguo@mail.iggcas.ac.cn¹GSA Data Repository item 2019276, detailed analytical and modeling methods and results, supplementary figures, and data tables, is available online at <http://www.geosociety.org/datarepository/2019/>, or on request from editing@geosociety.org.CITATION: Guo, Z. and Wilson, M., 2019, Late Oligocene–early Miocene transformation of postcollisional magmatism in Tibet: *Geology*, v. 47, p. 776–780, <https://doi.org/10.1130/G46147.1>

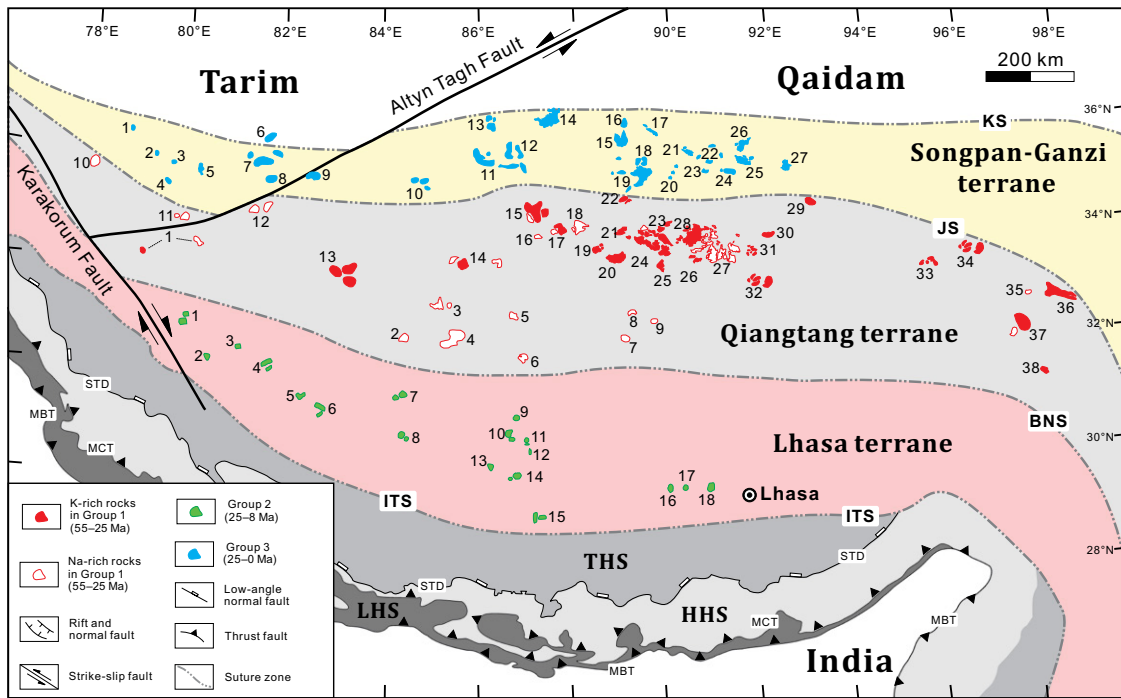


Figure 1. Distribution of postcollisional magmatic rocks on the Tibetan Plateau. Group 1 (55–25 Ma) formed in central Tibet; groups 2 (25–8 Ma) and 3 (25 Ma–present) are distributed in south and north Tibet, respectively. See Table DR4 (see footnote 1) for detailed locations of 91 samples collected in this study; names of volcanic fields correspond to numbers shown next to outcrops. BNS—Bangong-Nujiang suture; HHS—Higher Himalayan Sequence; ITS—Indus-Tsangpo suture; JS—Jinsha suture; KS—Kunlun suture; LHS—Lesser Himalayan Sequence; MBT—Main Boundary thrust; MCT—Main Central thrust; STD—South Tibetan detachment; THS—Tethyan Himalayan Sequence.

ing large ion lithophile element (LILE) concentrations from K-rich to Na-rich magmatic rocks (Fig. 3B). Sr-Nd-Pb isotopic modeling indicates that a carbonatitic component was present in their mantle source, consistent with carbonate sediments on the northward-subducted Indian passive continental margin being subducted into the sublithospheric mantle (Fig. 3C). The carbonatite component becomes weaker from the ultrapotassic and potassic magmatism through HKCA to ocean island basalt (OIB)-type magmas.

Group 2 rocks are K-rich magmatic rocks in south Tibet (Figs. 1 and 2B). They are distinguished from group 1 by low Sr/Nb ratios (Fig. 2C), enrichments of SiO₂ and K₂O (Fig. 2B), and depletion of Ca in olivine phenocrysts (Fig. 3A). The magmatic rocks display significant negative Sr-Ba anomalies in mantle-normalized trace-element patterns (Fig. DR4). These, together with Sr-Nd-Pb isotope mixing simulation results (Fig. 3C), indicate that a subducted Indian continental silicate sediment component was important in their mantle source, linking the petrogenesis of group 2 with northward Indian subduction.

Group 3 rocks are K-rich magmatic rocks (Fig. 2B) in north Tibet (Fig. 1). Intermediate and variable Ni/MgO and SiO₂ contents (Fig. 2D), together with Ca contents in olivine phenocrysts that span the boundary between silicate and carbonate metasomatism (Fig. 3A), indicate important roles for both carbonatitic and subducted terrigenous sediment components in their mantle source. The Sr-Nd-Pb isotope compositions plot between end members defined by depleted mid-oceanic ridge basalt (MORB) mantle (DMM), Asian continental lithosphere (ACL), and India-derived carbonate sediments (Fig. 3D), suggesting that ACL has subducted beneath north Tibet since 25 Ma (Fig. 4B).

These three groups of magmatic rocks are associated with different Tibetan terranes (Fig. 1), and they are typically located within the terranes, rather than along the terrane boundaries. The differences in the compositions of groups 1–3 resulted from the subduction of different types of continental lithosphere in a duality subduction system (Fig. 4).

DISCUSSION

Mantle Transition Zone-Derived Carbonated Mantle Plume

Petrogenesis of the mafic postcollisional magmas has been proposed to result from decompression-induced melting of upwelling asthenospheric mantle beneath central Tibet since 55 Ma (Guo et al., 2006). Their compositions may provide significant constraints on the nature and evolution of this mantle upwelling. The presence of CO₂-rich melt inclusions (Fig. DR3), the high-Ca contents in olivine phenocrysts (Fig. 3A), the occurrence of carbonatite-metasomatized mantle wehrlite xenoliths (Fig. DR5), distinct positive Sr-Ba anomalies in mantle-normalized trace-element patterns (Fig. DR4), and high proportions of carbonatitic components in the mantle source of group 1 (Fig. 3C) indicate upwelling of a carbonated upper-mantle plume, which originated from subducted Indian continental lithosphere and its cover of platform carbonate sediments arriving at the top of the mantle transition zone (MTZ) (Fig. DR6). Partial melting of this carbonated mantle resulted in group 1 magmatism from 55 to 25 Ma (Fig. 4A).

The magmatic rocks display a decrease in age (Fig. 2A), decreasing Ba/Th and Sr/Nb (Fig. 2C), and positive Sr-Ba anomalies in mantle-

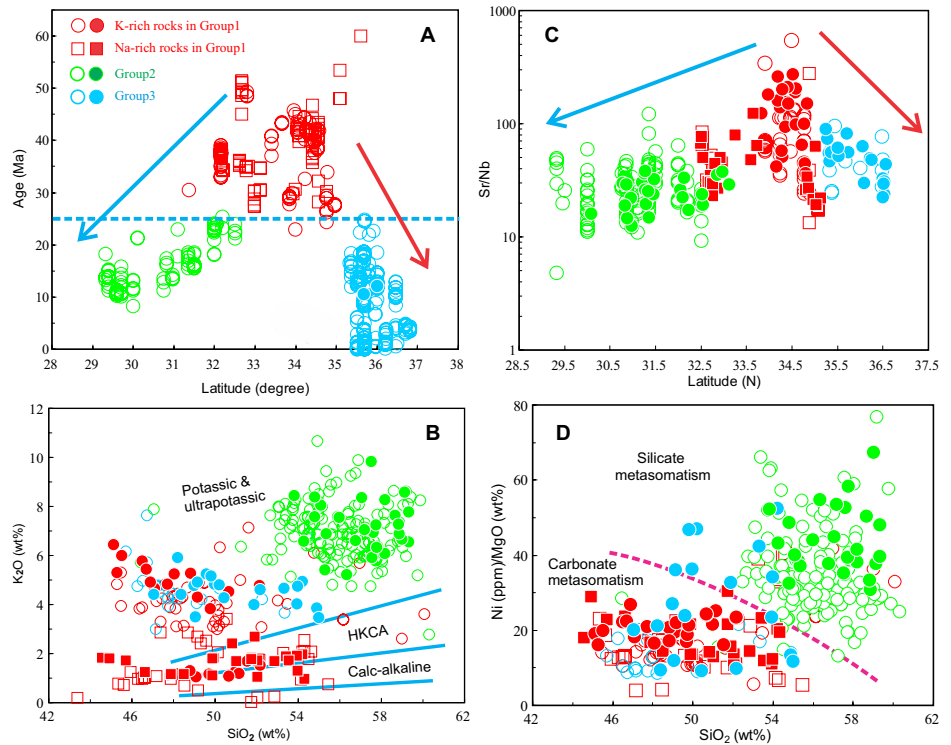
normalized trace-element patterns (Fig. DR4) from central (55–25 Ma) to south and north (25 Ma–present) Tibet. Both Na- and K-rich rocks are observed in the center of the proposed upwelling, but only K-rich rocks occur on its southern and northern margins (Fig. 2B). The transformation in their spatiotemporal distribution and compositions occurred at ca. 25 Ma, suggesting a decreasing proportion of the carbonated mantle component from the center (pre–25 Ma) to the margins (post–25 Ma) of the upwelling (Fig. 3C). There appears to have been a change in carbonated mantle plume (CMP) upwelling through time—a large-scale MTZ-derived CMP from 55 to 25 Ma (Fig. 4A), followed by a decrease in plume size after 25 Ma (Figs. 4B–4D).

The upwelling model is supported by recent geophysical studies. A high-electrical-conductivity and low-resistivity anomaly with a plume-like shape (Unsworth et al., 2004), together with a low-P wave velocity anomaly down to the MTZ (Nunn et al., 2014), has been recognized beneath central Tibet (Fig. DR6). These geophysical data clearly can only provide a present-day “snapshot” of our geochemistry-based model since 55 Ma. Despite the geophysical evidence for an upper-mantle plume-like structure, there is no large igneous province in Tibet, probably because there was no significant thermal anomaly (Guo et al., 2015), and the enriched component in the plume was carbonatitic (Fig. 3C).

Two-Stage Evolution Model

Continental subduction triggered both the CMP upwelling and the two-stage distribution of groups 1–3 (Fig. 2A). Thus, the history of group 1–3 magmatism could reflect a two-stage evolution of continental lithosphere subduction.

Figure 2. A: Age of postcollisional magmatic rocks on the Tibetan Plateau, indicating younging trends from central (group 1) to south (group 2) and north (group 3) Tibet, as shown by arrows. Blue dashed line indicates transformation of magmatism at 25 Ma. Filled and open symbols represent, respectively, data from this study (Table DR2 [see footnote 1]) and data published in previous studies (Table DR1). **B:** K_2O versus SiO_2 , HKCA—high-K calc-alkaline. **C:** Sr/Nb of postcollisional magmatic rocks, indicating decreasing trends of Sr/Nb from central (group 1) to south (group 2) and north (group 3) Tibet, as shown by arrows. This shows that carbonate melt metasomatism (with high Sr/Nb) occurred in mantle source of group 1 (55–25 Ma) in central Tibet, whereas silicate metasomatism (with low Sr/Nb) occurred in source of groups 2 and 3 (25 Ma to present) in south and north Tibet. Different trace-element ratios in south and north Tibet resulted from different compositions of silicate melt metasomatizing respective mantle sources, caused by different (dual) continental subduction. **D:** Ni (ppm)/MgO (wt%) versus SiO_2 (wt%), indicating group 1 resulted from carbonate-induced metasomatism, whereas group 2 was derived from a silicate sediment–melt metasomatized mantle source; roles for both carbonatitic and silicate melt metasomatism were recognized in mantle source of group 3 magmas. Pink dashed line separates fields of magmas derived from partial melting of mantle metasomatized by carbonate and silicate melts (from Guo et al., 2015). Filled and open symbols in B–D represent, respectively, data from this study (Table DR4) and data from previous studies (see source literature in the description following Table DR4).



The first stage formed a large-scale east-west-trending (group 1) magmatic belt in central Tibet from 55 to 25 Ma (Fig. 1), induced by a high proportion of India-derived carbonate sediments in its source (Fig. 3C). This resulted in CO_2 -fluxed melting of mantle peridotite above the subducted Indian slab (Fig. 4A), as evidenced by a series of

ultrapotassic and potassic to HKCA and OIB-like magmatic rocks (Fig. 2B). This first stage followed initial India-Asia collision at 65–60 Ma and the resultant northward subduction of the Indian plate with its cover of platform carbonate sediments (Kent and Muttoni, 2013) from 65 to 55 Ma; this lithosphere arrived at the top of the

MTZ beneath central Tibet at 55–50 Ma, based on the following evidence: (1) our Sr-Nd-Pb isotopic results identified subducted India-derived components in the group 1 source from 55 Ma (Fig. 3C); and (2) the presence of a thickened MTZ beneath central Tibet (Duan et al., 2017) is consistent with accumulation of a “cold” subducted

Figure 3. A: Ca (ppm) versus Fo (mole%) of olivine phenocrysts, indicating that group 1 resulted from carbonate metasomatism, whereas group 2 formed by silicate melt metasomatism of mantle source; group 3 is a result of both carbonatitic and silicate melt metasomatism. Red dashed line separates fields of olivine phenocrysts crystallized from melts of mantle metasomatized by carbonate and silicate melts (Ammannati et al., 2016). Filled and open symbols represent, respectively, data from this study (Table DR5 [see footnote 1]) and data from previous studies (see the description after Table DR5 for data sources). **B:** Compositional comparison (average) of carbonatite (Ying et al., 2004; Zhang et al., 2017) with group 1 magmas (Table DR4), indicating decreasing trend in trace-element contents from ultrapotassic and potassic, through high-K calc-alkaline (HKCA) to ocean island basalt (OIB)-type magmas in group 1. **C:** $(^{206}Pb/^{204}Pb)_i$ versus $(^{87}Sr/^{86}Sr)_i$, indicating three-component mixing model between depleted mid-oceanic ridge basalt (MORB) mantle (DMM), Indian carbonated melt, and Indian silicate melt in mantle source of groups 1 and 2. See Methods in the Data Repository for detailed modeling approach and results. Data sources and symbols are as in Figure 2B. **D:** $(^{206}Pb/^{204}Pb)_i$ versus $(^{87}Sr/^{86}Sr)_i$, indicating compositions of group 3 plot among three end members defined by DMM, Asian continental lithosphere (ACL), and India-derived carbonate sediments, suggesting that ACL has subducted beneath north Tibet since 25 Ma. Data sources and symbols are as in Figure 2B. See Methods in the Data Repository for data sources of ACL.

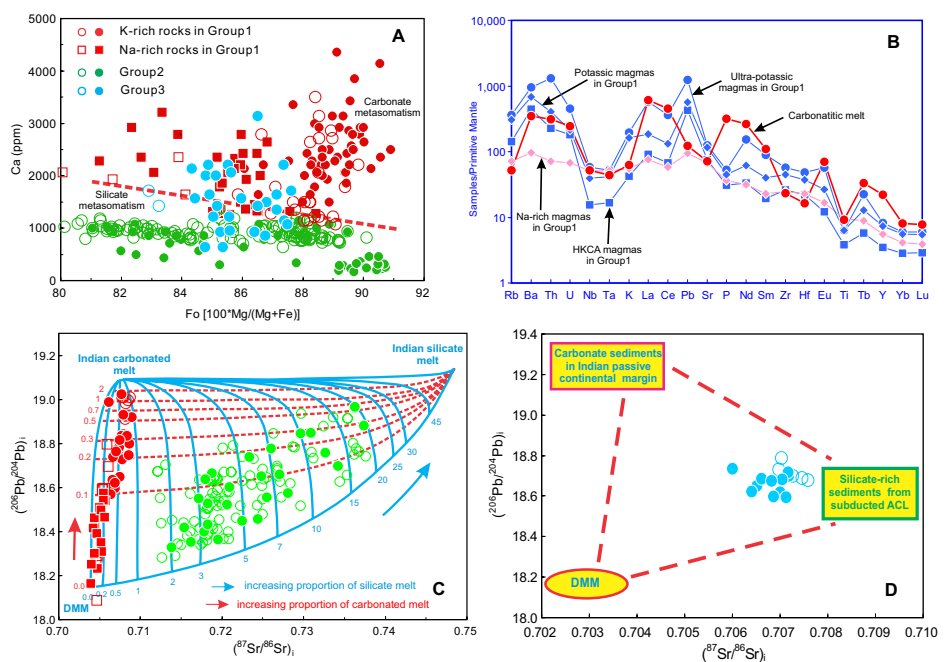
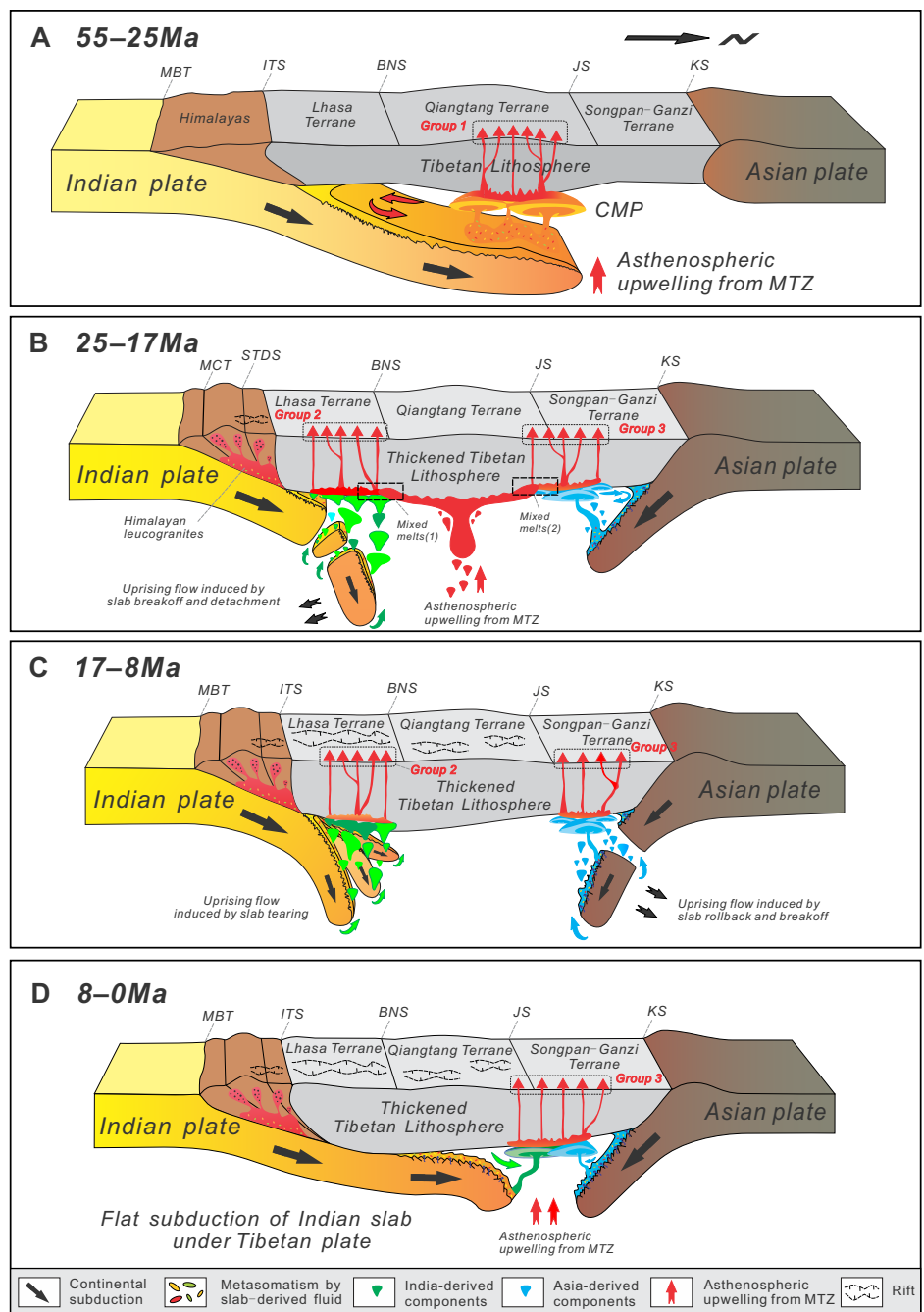


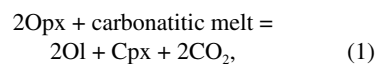
Figure 4. Model of two-stage evolution of post-collisional magmatism in Tibet (see Figure 1 for abbreviations). During the first stage (A), northward subduction of Neo-Tethys oceanic and Indian continental lithosphere beneath Tibetan Plateau caused upwelling of carbonate-rich asthenospheric mantle plume (CMP) from mantle transition zone (MTZ), leading to group 1 magmatism in central Tibet from 55 to 25 Ma. During the second stage from 25 Ma to present (B–D), dual convergent subduction systems of India and Asia continents resulted in silicate-melt metasomatism of mantle wedge beneath south and north Tibet. Groups 2 and 3 resulted from interaction between spreading of upwelling asthenospheric mantle plume head and silicate melts derived from subduction of continental sediments from 25 Ma to present. Subducted Indian slab rollback could have resulted in east-west-trending slab break-off since 25 Ma (Replumaz et al., 2016). This would have led to formation of a slab window, through which asthenospheric mantle flow triggered further melting of mantle source of group 2 (B). North-south extension resulted in the east-west-trending magmatic belt of group 2 from 25 to 17 Ma in south Tibet. North-south extension ceased at ca. 17 Ma and was replaced by east-west extension from 17 to 8 Ma (Williams et al., 2001; DeCelles et al., 2011), forming north-south-trending rifts in south Tibet and east-west extension by dike emplacement from 17 to 8 Ma (C). Northward flat subduction of Indian continental lithosphere resulted in the closure of the asthenospheric mantle window beneath south Tibet (Chen et al., 2018), leading to the absence of magmatism from 8 Ma to present (D). Group 3 comprised only small-scale potassic magmatism from 25 to 17 Ma (B), whereas an east-west-trending magmatic (including adakites; Wang et al., 2005) flare-up occurred in north Tibet from 17 Ma to present (C–D). This signals formation of a slab window due to rollback and break-off of the subducted Asian slab since 17 Ma (Guo et al., 2014), triggering melting of the metasomatized mantle wedge and its overlying thickened continental crust beneath north Tibet (C–D).



slab, which was the product of northward Indian lithosphere subduction. Thus, the MTZ beneath central Tibet, and overlying mantle metasomatized by an India-derived carbonate sediment component, can be considered to be a “graveyard” of subducted Indian lithosphere. Generation of low-density, low-viscosity carbonatitic melts with extreme enrichments in trace elements (Fig. 3B) is inferred to have induced upwelling of a carbonated upper-mantle plume from the MTZ beneath central Tibet since 55 Ma.

The ascent of carbonatitic melts in the mantle plume would result in their interaction with the surrounding mantle peridotite (Zhang et al., 2017). Orthopyroxene (Opx) is thought to have the highest efficiency and smallest enthalpy of reaction with ascending carbonatitic melts compared to other mantle minerals (Russell et al., 2012), and thus it is preferentially assimilated. Reaction rims on Opx in peridotite xenoliths indicate its dissolution during interaction within filtrating carbonatitic melts; this has been rec-

ognized in mantle wehrlite xenoliths entrained within postcollisional magmas to the northeast of the plateau (Fig. DR5). The interaction may be explained by following reaction:



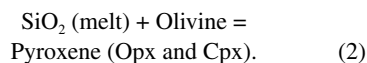
where Ol is olivine, and Cpx is clinopyroxene.

Continued reaction of Opx with ascending carbonatitic melts would result in a transition in magma compositions from carbonatitic to silicate melts. The transitions from carbonatite through K-rich to Na-rich magmatism in group 1 (Fig. 3B) are consistent with greater interaction between the carbonatitic melts and surrounding mantle rocks. We thus propose that the group 1 rock spectrum resulted from up-

welling of a carbonated upper-mantle plume beneath central Tibet from 55 to 25 Ma (Fig. 1).

The second stage (25 Ma to the present) is associated with occurrence of groups 2 and 3 in south and north Tibet. A subducted India-derived component has been identified in the source of group 2 (Fig. 3C), whereas an Asia-derived component has been recognized in group 3 (Fig. 3D). This indicates the occurrence of opposing Indian and Asian subduction systems during this period (Fig. 4B). This stage involved formation of a keel of thickened lithosphere in central Tibet (Wang et al., 2010) and a decreasing thickness of the lithosphere toward south and north Tibet, which resulted from lithosphere-asthenosphere interaction induced by mantle plume upwelling. The most important characteristics of this

stage, as a result of a gradual decrease of the India-Asia convergence rate (Jagoutz et al., 2015), was that magmatic activity weakened and finally ceased in central Tibet (Figs. 2A and 4C), because of the presence of thickened lithosphere (Wang et al., 2010), as well as the smaller scale of carbonated plume upwelling relative to that from 55 to 25 Ma. The decreasing lithospheric thickness would have led to edge-driven, small-scale convection in the plume head, which would have induced its southward and northward spreading (Fig. 4B). The southward spreading in the plume head, together with its interaction (labeled by mixed melts [1] in Fig. 4B) with SiO₂-rich mantle domains metasomatized by India-derived components (Guo et al., 2015), suggests that the source of group 2 was dominated by Higher Himalayan Crystalline Sequence (HHCS)-derived terrigenous components subducted within the mantle wedge beneath south Tibet (Fig. 4B). Similarly, interaction (labeled by mixed melts [2] in Fig. 4B) of northward spreading in the plume head with SiO₂-rich domains metasomatized by Asia-derived components (Guo et al., 2014) indicates that group 3 resulted from southward subduction of the Asian continent since 25 Ma (Fig. 4B). The discovery of mantle pyroxenite xenoliths in groups 2 and 3 (Wu et al., 2001; Cheng and Guo, 2017) suggests that their mantle source was influenced by silicate metasomatism according to the reaction:



Group 2 is characterized by an east-west-trending magmatic belt from 25 to 17 Ma (Fig. 4B), outcrops located within north-south-trending rifts from 17 to 8 Ma (Fig. 4C), and a lack of volcanism from 8 Ma to the present (Fig. 4D). This may be explained by slab break-off-induced north-south extension since 25 Ma (Replumaz et al., 2016), replaced by east-west extension from ca. 17 Ma (DeCelles et al., 2011) and northward flat subduction of Indian lithosphere leading to a closure of the mantle window since 8 Ma in south Tibet (Fig. 4D).

CONCLUDING REMARKS

The spatial distribution, volumes, and compositions of the postcollisional magmatic rocks in Tibet and their entrained mantle xenoliths indicate that the continental lithosphere-derived components in their mantle sources were different before and after 25 Ma, suggesting that a critical transformation in geodynamic processes occurred at ca. 25 Ma. The transition resulted from dual continental subduction becoming dominant since 25 Ma, which is a significant event in the evolution of the Tibetan Plateau. Magmatism prior to 25 Ma reflects the extensive contamination of the asthenosphere above the MTZ by northward-subducted Tethyan platform carbonate sediments.

ACKNOWLEDGMENTS

This study was supported by the Strategic Priority Research Program of the Chinese Academy of Sciences (grant XDB26000000), the Second Tibetan Plateau Scientific Expedition and Research (grant 2019QZKK0702), a grant from the Key Research Project of Frontier Sciences of the Chinese Academy of Sciences (grant QYZDY-SSW-DQC030), and a grant from the National Natural Science Foundation of China (grant 41772355). We thank M. Zhang, W. Zhao, and Z. Cheng for their help in this study. Catherine Mottram and two anonymous reviewers are acknowledged for their constructive reviews of an earlier version of the manuscript. We also thank the science editor, Dennis Brown, for his support.

REFERENCES CITED

- Ammannati, E., Jacob, D.E., Avanzinelli, R., Foley, S.F., and Conticelli, S., 2016, Low Ni olivine in silica-undersaturated ultrapotassic igneous rocks as evidence for carbonate metasomatism in the mantle: *Earth and Planetary Science Letters*, v. 444, p. 64–74, <https://doi.org/10.1016/j.epsl.2016.03.039>.
- Chen, J.-L., Yin, A., Xu, J.-F., Dong, Y.-H., and Kang, Z.-Q., 2018, Late Cenozoic magmatic inflation, crustal thickening, and >2 km of surface uplift in central Tibet: *Geology*, v. 46, p. 19–22, <https://doi.org/10.1130/G39699.1>.
- Cheng, Z., and Guo, Z., 2017, Post-collisional ultrapotassic rocks and mantle xenoliths in the Sailipu volcanic field of Lhasa terrane, south Tibet: *Petrological and geochemical constraints on mantle source and geodynamic setting: Gondwana Research*, v. 46, p. 17–42, <https://doi.org/10.1016/j.gr.2017.02.008>.
- DeCelles, P., Kapp, P., Quade, J., and Gehrels, G., 2011, Oligocene–Miocene Kailas Basin, southwestern Tibet: Record of post-collisional upper plate extension in the Indus-Yarlung suture zone: *Geological Society of America Bulletin*, v. 123, p. 1337–1362, <https://doi.org/10.1130/B30258.1>.
- DeCelles, P.G., Kapp, P., Gehrels, G.E., and Ding, L., 2014, Paleocene–Eocene foreland basin evolution in the Himalaya of southern Tibet and Nepal: Implications for the age of initial India-Asia collision: *Tectonics*, v. 33, p. 824–849, <https://doi.org/10.1002/2014TC003522>.
- Duan, Y., Tian, X., Liang, X., Li, W., Wu, C., Zhou, B., and Iqbal, J., 2017, Subduction of the Indian slab into the mantle transition zone revealed by receiver functions: *Tectonophysics*, v. 702, p. 61–69, <https://doi.org/10.1016/j.tecto.2017.02.025>.
- Guo, Z.F., Wilson, M., Liu, J.Q., and Mao, Q., 2006, Post-collisional, potassic and ultrapotassic magmatism of the northern Tibetan Plateau: Constraints on characteristics of the mantle source, geodynamic setting and uplift mechanisms: *Journal of Petrology*, v. 47, p. 1177–1220, <https://doi.org/10.1093/petrology/egl007>.
- Guo, Z.F., Wilson, M., Zhang, L.H., Zhang, M.L., Cheng, Z.H., and Liu, J.Q., 2014, The role of subduction channel mélanges and convergent subduction systems in the petrogenesis of post-collisional K-rich mafic magmatism in NW Tibet: *Lithos*, v. 198–199, p. 184–201, <https://doi.org/10.1016/j.lithos.2014.03.020>.
- Guo, Z.F., Wilson, M., Zhang, M.L., Cheng, Z.H., and Zhang, L.H., 2015, Post-collisional ultrapotassic mafic magmatism in south Tibet: Products of partial melting of pyroxenite in the mantle wedge induced by roll-back and delamination of the subducted Indian continental lithosphere slab: *Journal of Petrology*, v. 56, p. 1365–1406, <https://doi.org/10.1093/petrology/egv040>.
- Hu, X., Garzanti, E., Moore, T., and Raffi, I., 2015, Direct stratigraphic dating of India-Asia collision onset at the Selandian (middle Paleocene, 59 ±

- 1 Ma): *Geology*, v. 43, p. 859–862, <https://doi.org/10.1130/G36872.1>.
- Jagoutz, O., Royden, L., Holt, A.F., and Becker, T.W., 2015, Anomalous fast convergence of India and Eurasia caused by double subduction: *Nature Geoscience*, v. 8, p. 475–478, <https://doi.org/10.1038/ngeo2418>.
- Kent, D.V., and Muttoni, G., 2013, Modulation of Late Cretaceous and Cenozoic climate by variable drawdown of atmospheric pCO₂ from weathering of basaltic provinces on continents drifting through the equatorial humid belt: *Climate of the Past*, v. 9, p. 525–546, <https://doi.org/10.5194/cp-9-525-2013>.
- Nunn, C., Roecker, S.W., Tilmann, F.J., Priestley, K.F., Heyburn, R., Sandvol, E.A., Ni, J.F., Chen, Y.J., Zhao, W., and Team, I., 2014, Imaging the lithosphere beneath NE Tibet: Teleseismic P and S body wave tomography incorporating surface wave starting models: *Geophysical Journal International*, v. 196, p. 1724–1741, <https://doi.org/10.1093/gji/ggt476>.
- Replumaz, A., Funicello, F., Reitano, R., Faccenna, C., Balon, M., and Last, F., 2016, Asian collisional subduction: A key process driving formation of the Tibetan Plateau: *Geology*, v. 44, p. 943–946, <https://doi.org/10.1130/G38276.1>.
- Russell, J.K., Porritt, L.A., Lavallee, Y., and Dingwell, D.B., 2012, Kimberlite ascent by assimilation-fuelled buoyancy: *Nature*, v. 481, p. 352–356, <https://doi.org/10.1038/nature10740>.
- Unsworth, M., Wenbo, W., Jones, A.G., Li, S., Bedrosian, P., Booker, J., Sheng, J., Ming, D., and Handong, T., 2004, Crustal and upper mantle structure of northern Tibet imaged with magnetotelluric data: *Journal of Geophysical Research*, v. 109, B02403, <https://doi.org/10.1029/2002JB002305>.
- Wang, Q., McDermott, F., Xu, J.-F., Bellon, H., and Zhu, Y.-t., 2005, Cenozoic K-rich adakitic volcanic rocks in the Hohxil area, northern Tibet: Lower-crustal melting in an intracontinental setting: *Geology*, v. 33, p. 465–468, <https://doi.org/10.1130/G21522.1>.
- Wang, Q., Wyman, D.A., Li, Z.-X., Sun, W., Chung, S.-L., Vasconcelos, P.M., Zhang, Q., Dong, H., Yu, Y., Pearson, N., Qiu, H., Zhu, T., and Feng, X., 2010, Eocene north-south trending dikes in central Tibet: New constraints on the timing of east-west extension with implications for early plateau uplift?: *Earth and Planetary Science Letters*, v. 298, p. 205–216, <https://doi.org/10.1016/j.epsl.2010.07.046>.
- Williams, H., Turner, S., Kelley, S., and Harris, N., 2001, Age and composition of dikes in southern Tibet: New constraints on the timing of east-west extension and its relationship to postcollisional volcanism: *Geology*, v. 29, p. 339–342, [https://doi.org/10.1130/0091-7613\(2001\)029<0339:AACODI>2.0.CO;2](https://doi.org/10.1130/0091-7613(2001)029<0339:AACODI>2.0.CO;2).
- Wu, C., Yang, J., Li, H., Shi, R., and Men, F., 2001, Pyroxenite xenoliths in the volcanic rocks from North Tibet: *Acta Geoscientia Sinica (Diqui Xuebao)*, v. 22, p. 61–66, <https://doi.org/10.3321/j.issn:1006-3021.2001.01.012>.
- Ying, J., Zhou, X., and Zhang, H., 2004, Geochemical and isotopic investigation of the Laiwu-Zibo carbonatites from western Shandong Province, China, and implications for their petrogenesis and enriched mantle source: *Lithos*, v. 75, p. 413–426, <https://doi.org/10.1016/j.lithos.2004.04.037>.
- Zhang, G.L., Chen, L.H., Jackson, M.G., and Hofmann, A.W., 2017, Evolution of carbonated melt to alkali basalt in the South China Sea: *Nature Geoscience*, v. 10, p. 229–235, <https://doi.org/10.1038/ngeo2877>.

Printed in USA